Bull. ERS, No. 22(1989)

DYNAMIC BUCKLING BEHABIOURS OF RETICULATED SINGLE-LAYER DOME MODEL TO UP-AND-DOWN EARTHQUAKE EXCITATIONS

Tetuyuki TANAMI (1)
and
Yasuhiko HANGAI (2)

SUMMARY

Main purpose of this paper is the investigation of dynamic buckling behaviours of a reticulated single-layer dome model to the up-and-down earthquake excitations. The model using a flexible spring in each member is made weak in order to cause the dynamic buckling within the limited power of the shaking table. Dynamic properties of the model are studied by static loading tests of the members, free vibration tests and shaking table tests to the up-and-down earthquake excitations. Comparison of buckling loads of the model between tests and numerical results by using the static buckling analysis and the nonlinear response analysis are considered.

1. INTRODUCTION

Buckling problem of structures is classified into the static buckling problem and the dynamic buckling one. The dynamic stability problem has been studied because the various external forces to structures, such as wind and earthquake, act dynamically and there is a noteworthy fact that the buckling loads of spherical shells to step load are about a half of the corresponding static buckling loads as shown in Fig.1.

Shell has been used as a roof structure covering large space without columns from ancient times. Nowadays, space frame which is a descrete structure with curved surface is often used because of its light weight. Double-layer or multi-layer space frames are usually adopted in order to achieve stiffness and strength for large span. But in small scale within the base diameter of 50m, a few kinds of single-layer arrangement are often adopted from constructional and economical points of view. As compared with the former, the characteristics of single-layer are existed in the strong dependence on the geometrically nonlinearity. Therefore, in the case of the reticulated singe-layer dome, it is important to investigate the elastic stability problem. There are many research papers and survey papers about the static buckling problem of space frames (Ref.1,2). But, there are few studies on dynamic buckling problem of space frame to earthquake excitations.

Static loading tests of the members, free vibration tests and shaking table tests to the up-and-down excitations by using sine waves and quasi-earthquake waves are carried out in the present paper in order to investigate the dynamic properties of a reticulated single-layer dome model with pin-connected joints, besides the comparison of buckling loads between the present tests and the numerical results by using the static buckling analysis and the nonlinear response analysis. In order to grasp

---

(1) Research Associate, Institute of Industrial Science, University of Tokyo, JAPAN
(2) Professor , Institute of Industrial Science, University of Tokyo, JAPAN

the dynamic buckling behaviours within the limited power of the shaking table, the weak model using a flexible spring in each member is used for the tests.

2. MODEL AND PROPERTIES OF MEMBER

Fig.2 shows the configration of a reticulated single-layer shallow dome model with triangular unit. The model is composed of 132 members pin-connected at 61 joints. Base diameter(a), rise(H), semi-open angle(θ) and rise-to-span ratio (H/a) of the model are 2.8m, 37.5cm, 30° and 0.135, respectively. There are 10 kinds of members between the lengths of 36.5cm and 48.6cm, and the mean length is 40.6cm, in which the length means the distance between the corresponding joints. Photo.1 shows the model installed on the shaking table. Effectiveness of shaking table tests by using the similar model was examined before as given in Ref.(3). In the present study, more weak model is used in order to reveal the dynamic buckling to the up-and-down earthquake excitations.

Fig.3 and Photo.2 denote the detail of a typical member, which is composed of steel spring and two brass tubes with slightly different diameters. Photo.3 shows the completely pin-connected members at a joint with the weight of 109gf. First, the compression and tension tests are carried out to estimate the spring constant (k) and the extensional rigidity (EA) of members under the static load. Typical load-displacement relation is given in Fig.4, in which the curves are relatively irregular at the first or the secont loading step because of the friction between spring and other parts. Total weigth for the loading is 8 kgf at intervals of 0.5 kgf. Table 1 shows (k),(EA) and the measured length (L) of twelve members. Stiffness in tension side is smaller than in compression side, though the tendency is not so clear as the member is long. Mean values of (k),(EA) and (L) are 41.7 cm, 13.06 kgf/cm and 533.1 kgf, respectively.

3. TESTS ON DYNAMIC LOADINGS

Fig.5 shows the installed positions of 11 accelerometers. CH.1 is on the shaking table for recording input accelerations, and the remainders (CH.2 to CH.11) are used for recording the time histories of response accelerations in the normal direction at each joint at the sampling interval of 1/50 sec. Response displacement is also measured at the crown of the model , in which the responses to the inward direction of the model are expressed by plus. In the figure, three circles denote the loading positions for free vibration tests mentioned in the following section. C0,C1,C2,C3 and C4 illustrate the center of model and four concentric circles, respectively, as shown in Fig.6. And then, it follows that the six accelerometers (CH.3 to CH.8) belong to C2.

3.1 SINE WAVE EXCITATION TESTS

Dynamic behaviours of the model to the up-and-down earthquake excitations of sine waves in the region from the linear to the buckling responses are tested. There are 10 kinds of input acceleretion levels for the sine wave excitations and the distinction of the levels is represented by SIN01,SIN02,SIN03,SIN04,,,,,SIN10. Maximum input accelerations to each input level are shown in Table 2 , in which the difference of maximum input accelerations to both the directions is due to the power of the shaking table.

Frequency of the sine wave was fixed in 4.0 Hz and the model buckled

dynamically at the input level of SIN10. Let us consider the results obtained through the tests in the following.

Fig.7 shows time histories of response accelerations at the positions of CH.1,CH.2 and CH.6 with the input levels of SIN04,SIN09 and SIN10. Enlargement of the response accelerations to the input acceleration of CH.1 is remarkable at the crown of CH.2. And, when the level of input accelerations increases, the appearance of higher components of frequencies is found out in the figure. These components are manifest from the Fourier spectrum analyses to the input levels of SIN04,SIN09 and SIN10 as shown in Fig.8. Although the input acceleration with fixed frequency component of 4 Hz certainly contains other components at the positions of integer-fold of 4 Hz because of the properties of the shaking table, the corresponding higher harmonic components to the input frequency of 4 Hz are so prominent as increasing the input level as shown in the response accelerations at CH.2 and CH.6. The lower harmonic component to input frequency of 4 Hz is also found out in the figure. To examine these higher and lower components, depending on the strong geometrically nonlynearity of stiffness of the model, is necessary for well understanding to the dynamic properties of the model.

Fig.9 shows the variations in the magnifications of the response accelerations (CH.2 to CH.11) to the input accelerations (CH.1) separately with each maximum value to both the directions by using every input level from SIN01 to SIN10, in which the magnification is simply estimated by dividing the maximum response acceleration by the maximum input acceleration of CH.1. Interesting behaviours are shown in the figure except the rigid body motion at the first input level of SIN01 with the maximun acceleration of around 100 gals. Namely, CH.3 to CH.8 on C2 and CH.9 and CH.11 on C3, in which C2 and C3 are illustrated in Fig.6, show the linear stationary responses of the model between the input level of SIN02 and SIN09. And CH.10 on C1 and CH.2 on C0 keep the stationary responses in the input level over SIN03 (or SIN04) and over SIN05 (or SIN06), respectively. Hence, it will be possible to say that the response behaviours of the model to the up-and-down excitations are so insensible as being close to the crown of the model and the model becomes the stationary responses in the level of around 350 gals.

Restoring force of the model which is examined by measuring the height of the model at the crown after every excitation as tabulated in Table 3 is good enough except the measured value after the input level of SIN09. The model buckled dynamically and slowly at the input level of SIN10. The progress of buckling is shown in Photo.4 as a series of photographs.

3.2 FREE VIBRATION TESTS

In this section, the dynamic properties of the model, such as natural period and damping factor are investigated. Free vibrations are caused by cutting a string which supports the weight of 2625 gf at the crown(CH.2) or the eccentric positions(CH.6 and CH.10) as shown by circles in Fig.5.

Although the estimasion of damping factor is difficult because of the extremely rapid decrease of time histories of response accelerations, Fig.10 illustrates the results obtained by using all of useful data. The estimated damping factor (h) are marked by circles in the figure, in which <x> means the damping factors which are estimated at the loading positions. Number of the same values in the estimated damping factors is also classified by using bar graphs in the low position of the figure, in which the painted parts corresponding to <x> are excluded from the estimation of damping factor of the model because damping factor at the

loading position tends to be overestimated. As the results, the damping factor (h) and the natural period (T) of the model obtained by free vibration tests are roughly 0.2 ± 0.05 and 0.4 ± 0.2 sec, respectively.

3.3 EARTHQUAKE EXCITATION TESTS

Three quasi-earthquakes of "10/4(1),(2)", "11/6(1),(2)" and "12/17(1),(2)" with the dominant components at 8.52 Hz, 8.50 Hz and 8.30 Hz, respectively, as shown in Table 4, in which (1) and (2) showing the difference in input levels are used as the input data to the shaking table in order to investigate the response behaviours of the model.

Time histories of input and response accelerations, Fourier spectra of input and response accelerations, and spectrum ratios of response accelerations to input accelerations are shown in Figs.11(a),(b),(c), Figs.12(a),(b),(c) and Figs.13(a),(b),(c), respectively, in which (a),(b) and (c) correspond to the names of quasi-earthquakes of "10/4", "11/6" and "12/17", respectively. In some time histories in Fig.11, for example, in the case of 10/4(2) in Fig11(a), small and large amplitudes appear irregularly. This can be understood from the response behaviours due to the sine wave excitations given in Fig.9, where small amplitudes as a rigid body motion of the whole model are caused by the lower excitation level, and large amplitudes as an elastic motion appear in the region of the comparatively high excitation level. In the case of earthquake excitation, these small and large amplitudes are irregularly caused based on the time histories of input level. This is also observed in the spectrum ratios of Fig.13, where the model nearly behaves as a rigid body in the cases of 10/4(1) and 11/6(1) and 11/6(2).

The magnifications of response acceleration, defined by the ratios of the maximum response acceleration to the maximum value of input acceleration, are shown in Figs.14(a),(b) and (c), in which Fig.14(a) shows the difference in the magnifications between 10/4(1) and 10/4(2) to both the directions separately. Similarly, Figs.14 (b) and (c) correspond to the cases of 11/6 and 12/17, respectively. The model behaves as a rigid body motion under the input level of 10/4(1) and behaves as an elastic motion under the input level of 10/4(2), then the straight lines connecting the corresponding magnifications between 10/4(1) and 10/4(2) go up to the right. The same relation is shown in the relation between 11/6(1) and 11/6(2), but in the case of 12/17, the straight lines go horizontally since the model under the input level of 12/17(1) already behaves as an elastic motion. Fig.15 shows the time histories of response accelerations under the input levels of 12/17(1) and 12/17(2).

3.4 RESONANCE CURVES

Sweep tests are carried out in order to obtain the resonance curves expressed by the magnifications of response accelerations (CH.2 to CH.11) to the input level on the shaking table (CH.1) within the region lower than the frequency of 42 Hz by the up-and-down stationary sine wave excitations, of which the maximum acceleration is a fixed value of 100 gals. Fig.16 shows the resonance curves of CH.2 on C0, CH.10 on C1, the average of from CH.3 to CH.8 on C2 and the average between CH.9 and CH.11 on C3, respectively. From this figure, the accurate resonance point cannot be found out.

4. NUMERICAL ANALYSIS

First, the extensional rigidity is estimated by using the spring

constant obtained by the static loading test of the member described in Chapter 2. Then, the free vibration analysis, the static buckling analysis and the nonlinear response analysis under the stationary sine wave earthquake excitation are carried out in order to compare with test results.

4.1 EXTENSIONAL RIGIDITY (EA)

Spring constants(k) of twelve members are already shown in Table 1. Extensional rigidity (EA) can be estimated by using these spring constants as

$$(EA) = (k) \times (\text{member length}).$$

Since the model has a lot of kinds of members with different member length, the average length obtained by measuring the lengths before each test is used to estimate the extensional rigidities, which are given in Table 5.

4.2 FREE VIBRATION ANALYSIS

The natural frequencies for 111 components between 1.58 Hz and 36.4 Hz are obtained by the eigen-value analysis using the extensional rigidity of 419.1 kgf and the consistent mass. The results are shown in Fig.17 as a histogram of distribution of natural frequencies. The first two mode shapes are asymmetrical and the first axisymmetrical mode shape appears in the third with the natural frequency of 1.685 Hz which means the natural period of 0.593 sec. Fig.18 shows the first six natural frequencies and the correspondig mode shapes among twelve axisymmetrical components.

The first natural frequencies obtained between free vibration tests and eigen-value analysis are 0.6 ± 0.2 sec and o.593 sec , respectively. These values are well coincident with test results. And, the tendency obtained from the histogram of distribution of natural frequencies in Fig.17 is similar to the spectrum ratios obtained by earthquake excitation tests in Fig.13 and the resonance curves obtained by sweep tests in Fig.16.

4.3 NONLINEAR ANALYSES

Firstly, the static buckling analysis is carried out in order to compare the difference of buckling loads obtained under the static load and the dynamic load. The buckling load to conical load distribution is also estimated by the static buckling analysis in addition of the case of the uniform load because the equivalent static loads of the single-layer dome to the up-and-down earthquake excitations are similar to the conical load distribution as shown in Ref(4).

Figs.19 and 20 show the load-displacement relations which lead to the buckling loads of 6.23 kgf and 1.84 kgf for the uniform load and the conical load distribution , respectively. The ratio of the buckling load for the conical load distribution to the uniform load is about 30 percents. Figs.21 and 22 show the progress of the buckling under the uniform load and the conical load obtained by using the deflection mode shapes, respectively. The response behaviours observed from the preceding tests under sine wave excitations are similar to the buckling mode to the conical load distribution. The corresponding buckling load to a different extensional rigidity is estimated by using the linear relation between the buckling load and the extensional rigidity as shown in Fig.23.

Secondly, the nonlinear response analysis of the model to the sine wave earthquake excitation with the fixed frequency of 4 Hz and the maximum acceleration of 300 gals is carried out. Figs.24(a) and (b) show the time histories of response accelerations and the time histories of

response displacements, respectively. In this case with the input acceleration of 300 gals, the model reveals the dynamic buckling. Appearance of the higher components of frequency over 4 Hz, which is found out in Fig.8 based on the tests of sine wave excitations, is similarly recognized in the numerical results of the time histories of response accelerations. Fig.25 shows the transition of deflection modes. The mode shape at the nondimensional time of 4.0 is similar to the static buckling mode under the conical load distribution.

Table 5 shows the comparison of the buckling loads between the static buckling analysis and the nonlinear response analysis. Dynamic buckling load (TEST.DBL) by the tests under sine wave excitations with the fixed frequency of 4 Hz is simply estimated as the total weight of 89.3 kgf in the following expressions.

$$\begin{aligned} \text{TEST.DBL} &= \text{Total Weight} \times \text{Input acceleration} / g \\ &= 89.3 \times 579 / 980 = 52.7 \text{ kgf}, \end{aligned}$$

where the input acceleration of 579 has been estimated by the average of 534 and 624 gals for SIN09 and SIN10, and (g) is the acceleration of gravity.

When the dynamic properties of the model are taken into consideration, the buckling load(TEST.DBL) must be overestimated because the model behaves as a rigid body within about 100 gals and occurs the elastic responses over about 350 gals, then the actual buckling loads may be existed between 43.6 kgf and 20.9 kgf, respectively, as shown in the following expressions.

$$\begin{aligned} \text{TEST.DBL(1)} &= 89.3 \times (579 - 100) / 980 \\ &= 43.6 \text{ kgf}, \end{aligned}$$

and

$$\begin{aligned} \text{TEST.DBL(2)} &= 89.3 \times (579 - 350) / 980 \\ &= 20.9 \text{ kgf}. \end{aligned}$$

Static buckling loads of the model under the uniform load and the conical load distribution with the (EA) of 533.1 kgf are 7.92 kgf and 2.34 kgf, respectively, since the buckling loads to the (EA) of 405.3 kgf are already known and the (EA) is in proportion to the buckling load as shown in Fig.23. In the case of nonlinear response analysis, the slightly weak model with the (EA) of 419.1 kgf buckles at the input acceleration of 300 gals, therefore, the dynamic buckling load is estimated within 27.3 kgf.

5. CONCLUSION

In the paper, the dynamic buckling behaviours of reticulated single-layer shallow domes to up-and-down excitation are investigated by test and analysis in order to compare with the static buckling behaviours. For a model, members using a flexible spring in each member and pin-connected joints are newly developed in order to cause the dynamic buckling within the limited power of the shaking table.

Free vibration tests, vibration tests under sine wave excitations as well as earthquake excitations are carried out, and the geometrically non-linear analysis is also used to obtain the static buckling load. Then, results by both test and numerical analysis are compared with. As a result, it is shown that the load distribution is an important factor when the dynamic buckling load is estimated by the static buckling analysis.

6. REFERENCES

(1) The Task Committee on Latticed Structures of the Committee on Metals of the Structural Division,"Latticed Structures: state-of-the-art Report," Journal of the Structural Division, ASCE, Vol.102,No.ST11,November 1976

(2) IASS Working Group on Spatial Steel Structures," Analysis,Design and Realization of Space Frames; a State-of-the-Art Report,"Bulletin of the International Association for Shell and Spatial Structures,n.84/85, Vol. XXV-1/2,1984.

(3) TANAMI,T. and HANGAI,Y.,"Shaking Table Tests for the Dynamic Behaviours of Reticulated Single-Layer Dome by Use of a Spring Model," Proceeding of ICSB, Oct.27-30,1987, Beijing CHINA, pp441-448.

(4) TANAMI,T.,TAKI,S. and HANGAI,Y., "Structural Behaviours of Single-Layer Frames (Parts 3) Dynamic Buckling of Pin-connected Single-layer Domes," Monthly J. of I.I.S.,University of Tokyo, Vol.40,No.12,1988,pp21-24 (in Japanese)

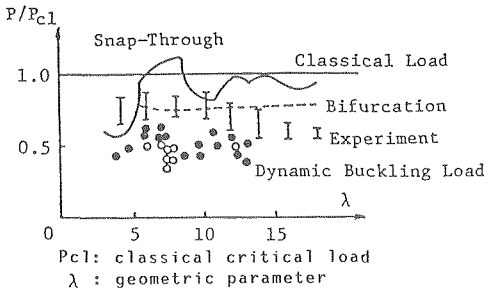

FIG.1: Comparison of Buckling Loads of Spherical Caps

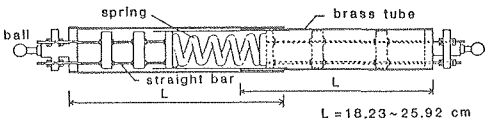

FIG.3: Detail of Member

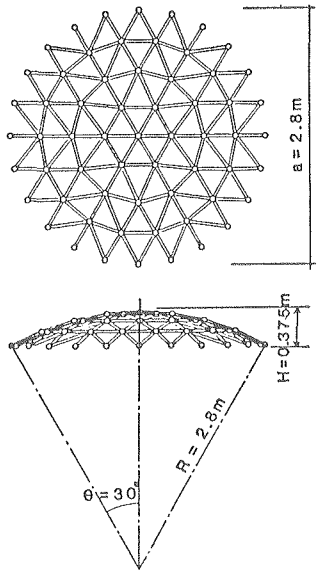

FIG.2: Reticulated Single-Layer Model

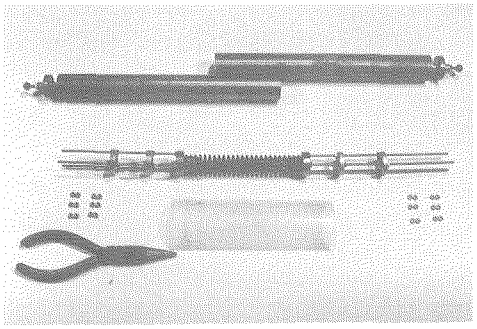

PHOTO.2: Parts of a Member

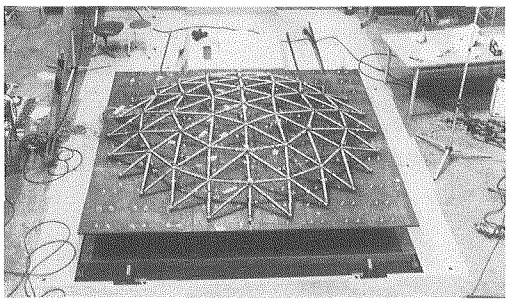

PHOTO.1: Model on Shaking Table

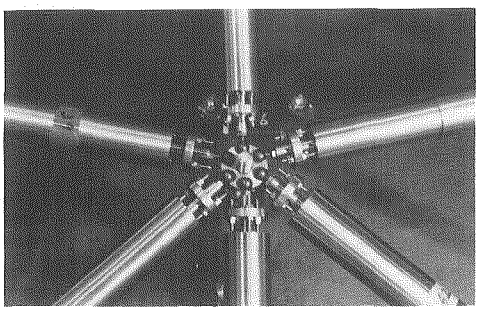

PHOTO.3: Pin-Connected Joint

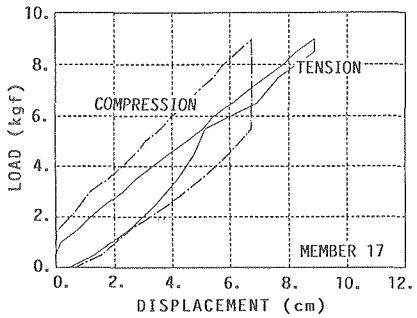

FIG.4:
Load-Displacement Relation of Member

TABLE 1: Spring Constant (k)

NO	L(cm)	k (kgf/cm)		EA (kgf)	
		TENSION	COMPRESSION	TENSION	COMPRESSION
1	36.2	16.5	22.0	598.0	794.7
84	37.5	14.3	24.9	535.7	932.2
37	37.6	8.3	9.3	311.3	350.9
107	38.0	12.8	27.2	487.9	1034.6
46	39.6	11.2	13.6	441.6	539.2
61	39.6	10.9	16.3	433.3	644.1
17	45.6	9.8	10.2	448.7	466.1
26	45.9	9.9	11.7	455.6	537.4
94	42.6	9.5	11.1	405.6	473.7
130	42.1	11.5	15.7	486.0	662.3
57	47.9	10.5	9.6	501.7	459.9
67	48.1	7.5	9.0	358.4	434.1
AVE.	41.7	13.1	15.0	455.3	610.8

NO : NUMBER OF MEMBER
L : MEASURED LENGTH BETWEEN THE CORRESPONDING NODES
k : SPRING CONSTANT EA : EXTENSIONAL RIGIDITY

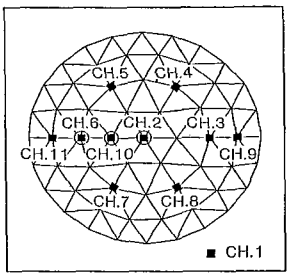

FIG.5: Installed Positions of Accelerometers

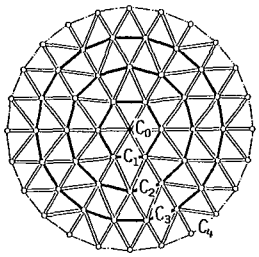

FIG.6: Explanation of C0,C1,C2,C3 and C4

TABLE 2: Maximum Input Accelerations in the case of SINE WAVE Excitations

SINE-WAVE of 4 Hz		SIN01	SIN02	SIN03	SIN04
MAXIMUM INPUT ACCELERATION (GAL)	PLUS	88	172	215	252
	MINUS	-93	-190	-250	-310

SIN05	SIN06	SIN07	SIN08	SIN09	SIN10
292	342	400	451	534	624
-373	-433	-490	-561	-679	-796

TABLE 3: Restoring Force of Model (CM)

PRE-TEST	SIN01	SIN02	SIN03	SIN04	SIN05
0.0	***	***	-0.1	0.0	***

SIN06	SIN07	SIN08	SIN09	SIN10
-0.1	-0.1	***	-0.9	BUCKLING

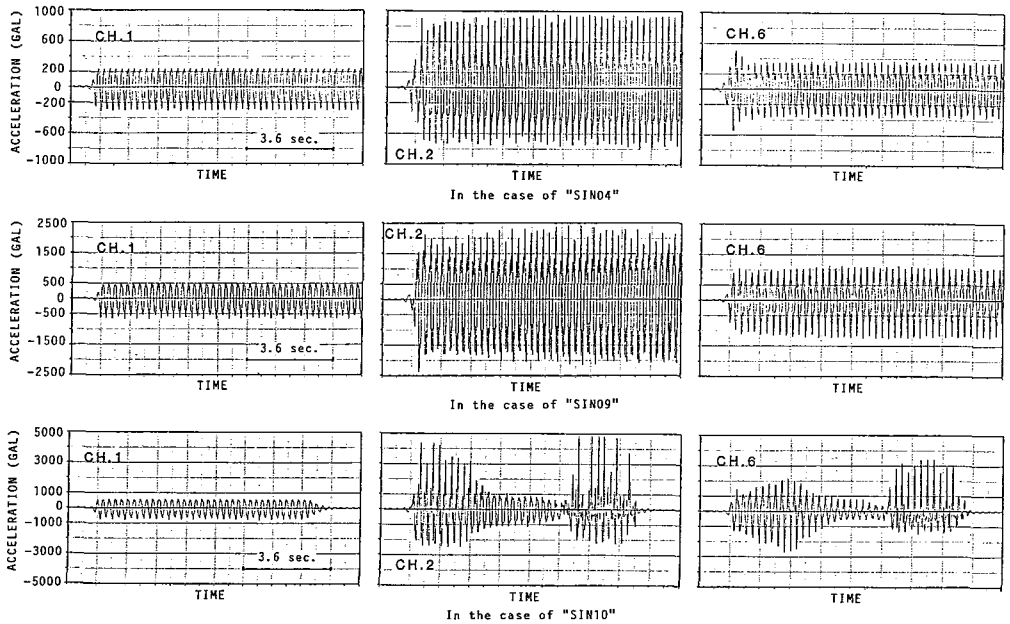

FIG.7: Time Histories of Response Accelerations at CH.1, CH.2 and CH.6 to "SIN04," "SIN09" and "SIN10"

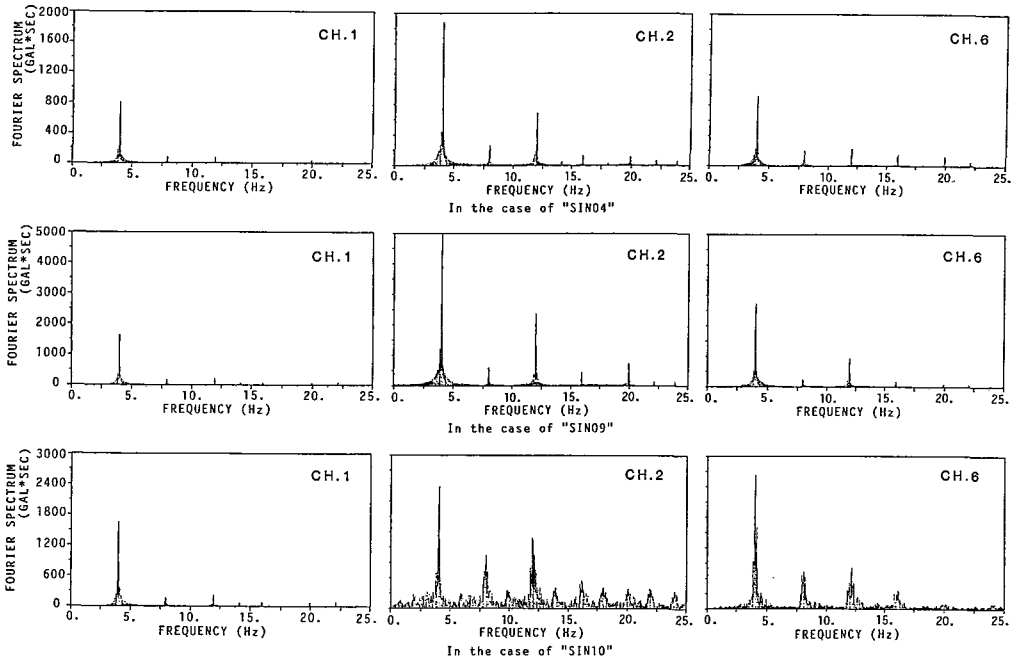

FIG.8: Fourier Spectra of Response Accelerations at CH.1, CH.2 and CH.6 to "SIN04," "SIN09" and "SIN10"

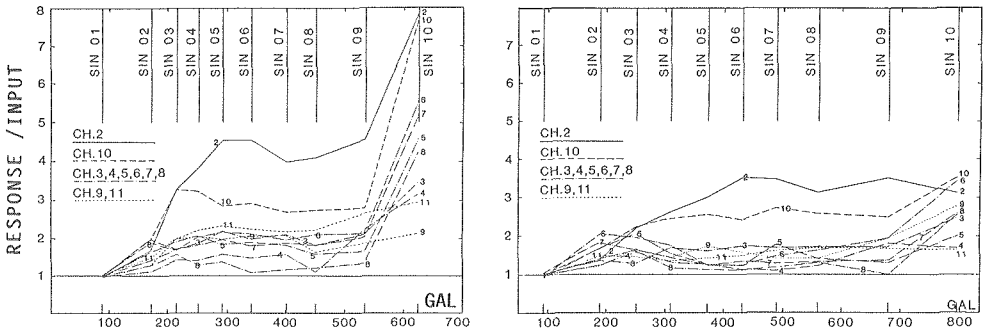

FIG.9: Relations between Magnification of Response Accelerations and Input Accelerations in the case of SINE WAVE EXCITATIONS

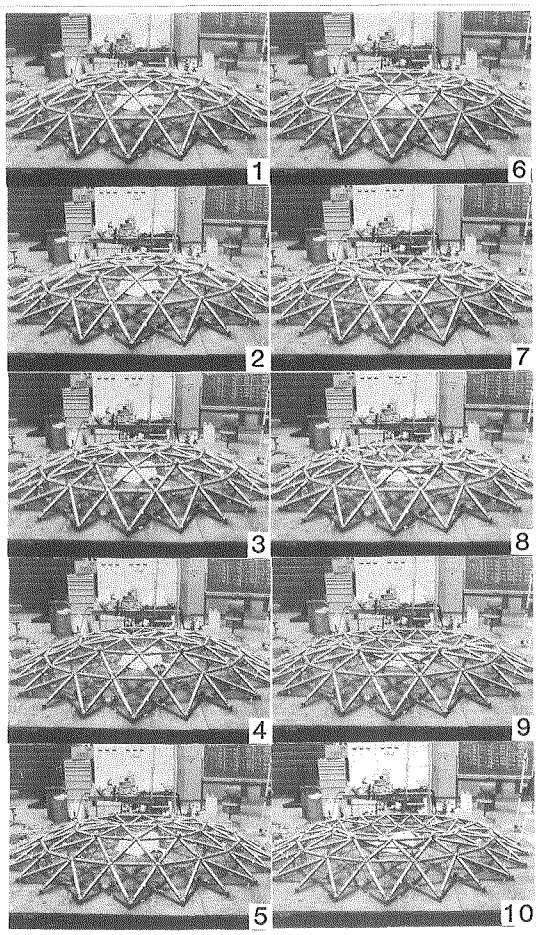

PHOTO.4: Progress of Dynamic Buckling

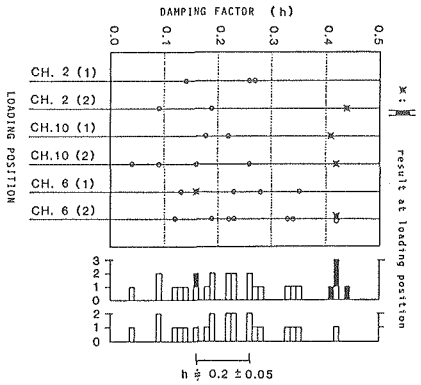

FIG.10: Estimation of Damping Factor

TABLE 4: Dimensions of Input Earthquake Accelerations

INPUT TYPE	INPUT LEVEL (1)		
	ACCELERATION(GAL)		FREQUENCY
	MAX.	MIN.	(Hz)
10/ 4	208	206	8.52
11/ 6	130	110	8.50
12/17	288	291	8.30

INPUT TYPE	INPUT LEVEL (2)		
	ACCELERATION(GAL)		FREQUENCY
	MAX.	MIN.	(Hz)
10/ 4	450	527	8.52
11/ 6	336	329	8.50
12/17	504	594	8.30

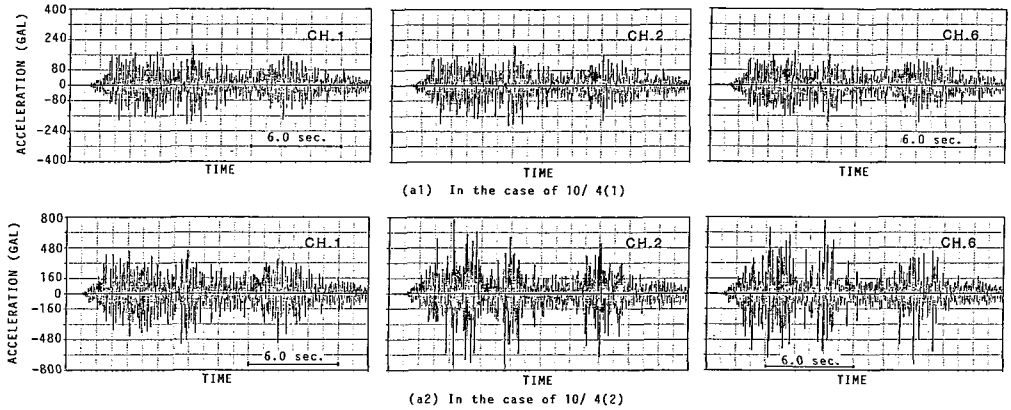

FIG.11(a): Time Histories of Response Accelerations at CH.1,CH.2 and CH.6 to "10/ 4"

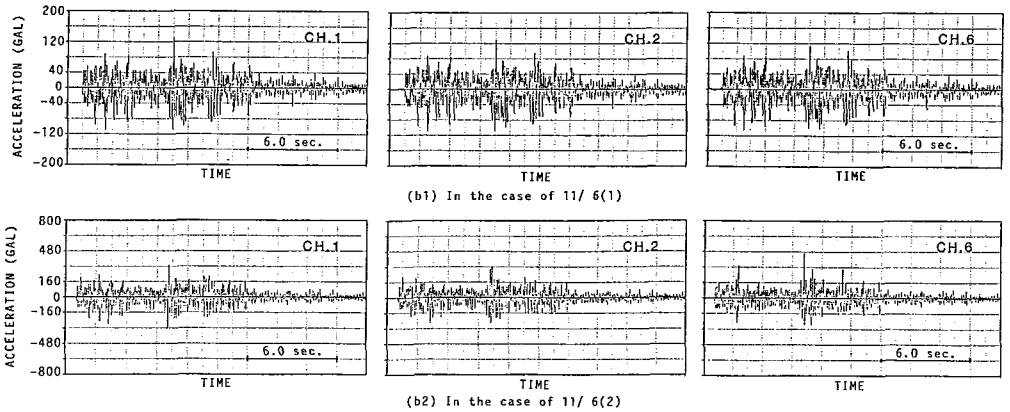

FIG.11(b): Time Histories of Response Accelerations at CH.1,CH.2 and CH.6 to "11/ 6"

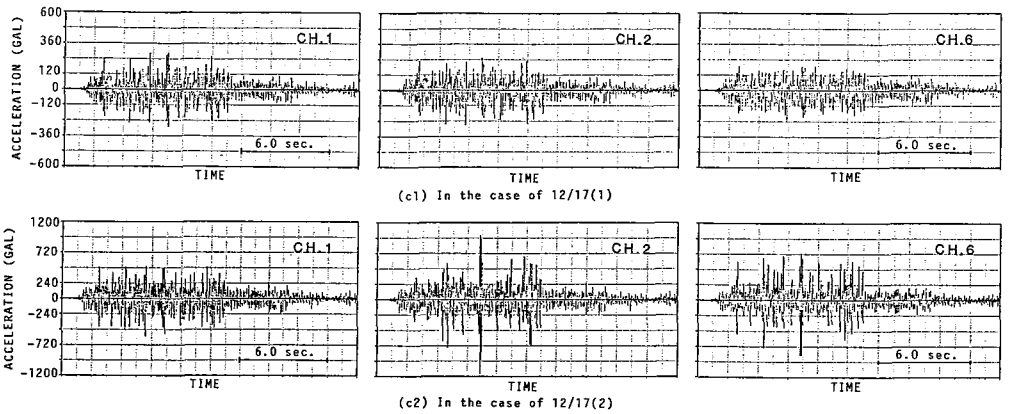

FIG.11(c): Time Histories of Response Accelerations at CH.1,CH.2 and CH.6 to "12/17"

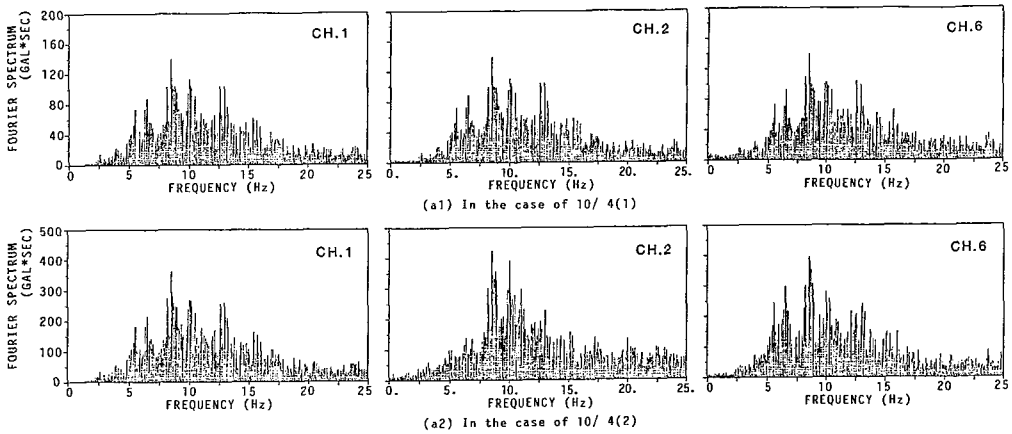

FIG.12(a): Fourier Spectra of Response Accelerations at CH.1 CH.2 and CH.6 to "10/ 4"

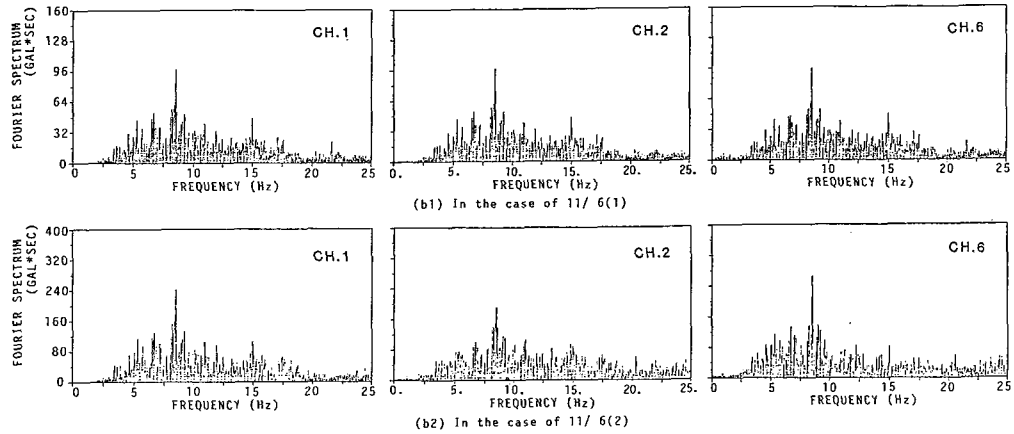

FIG.12(b): Fourier Spectra of Response Accelerations at CH.1,CH.2 and CH.6 to "11/ 6"

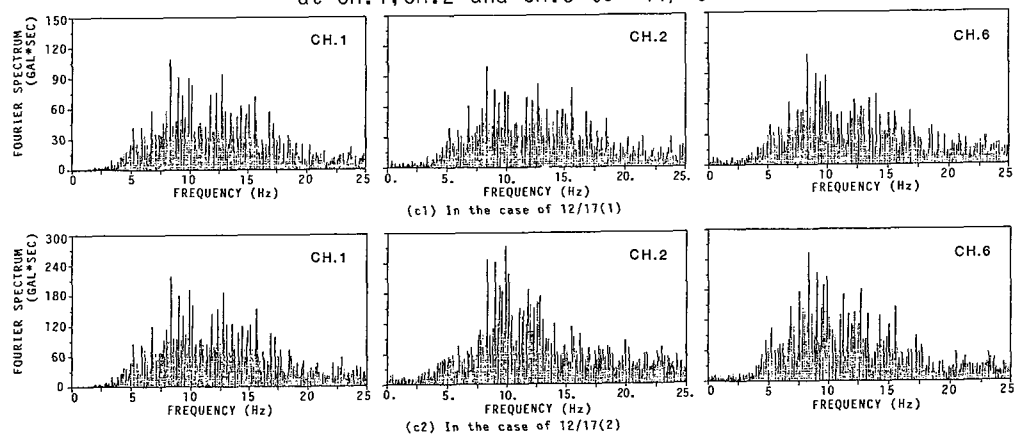

FIG.12(c): Fourier Spectra of Response Accelerations at CH.1,CH.2 and CH.6 to "12/17"

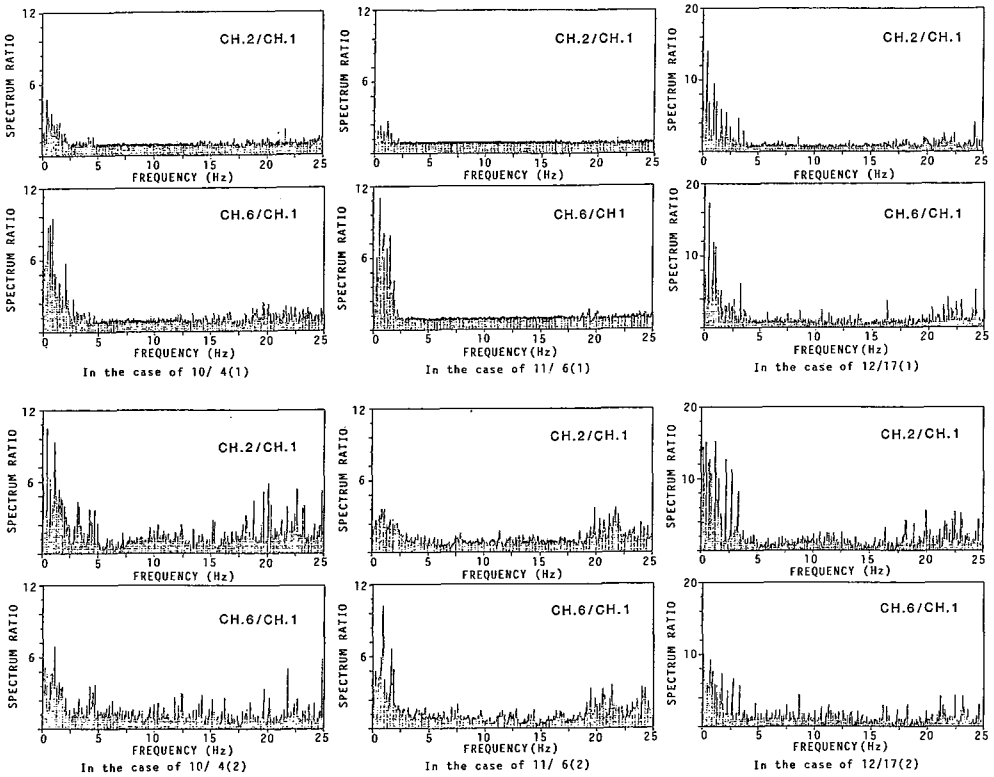

FIG.13(a): Spectrum Ratios at CH.2 and CH.6 to "10/ 4"

FIG.13(b): Spectrum Ratios at CH.2 and CH.6 to "11/ 6"

FIG.13(c): Spectrum Ratios at CH.2 and CH.6 to "12/17"

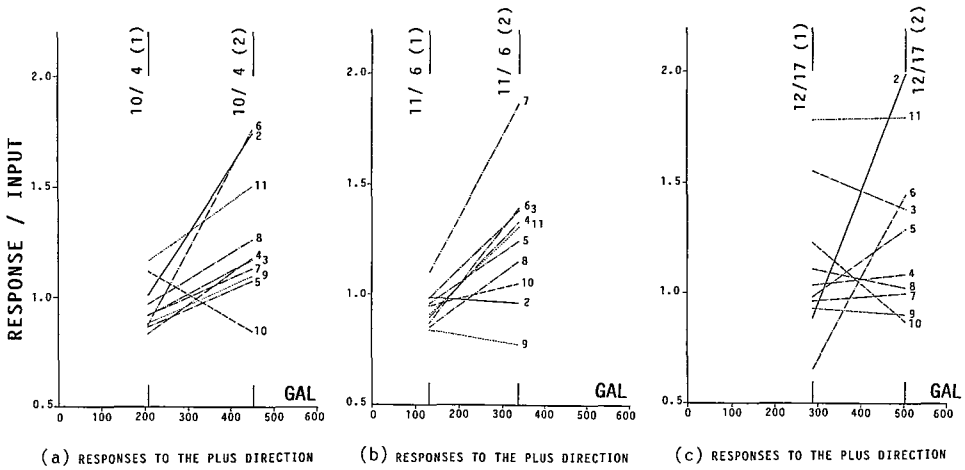

FIG.14-1 : Magnifications of Response Accelerations in the case of "EARTHQUAKE EXCITATIONS"

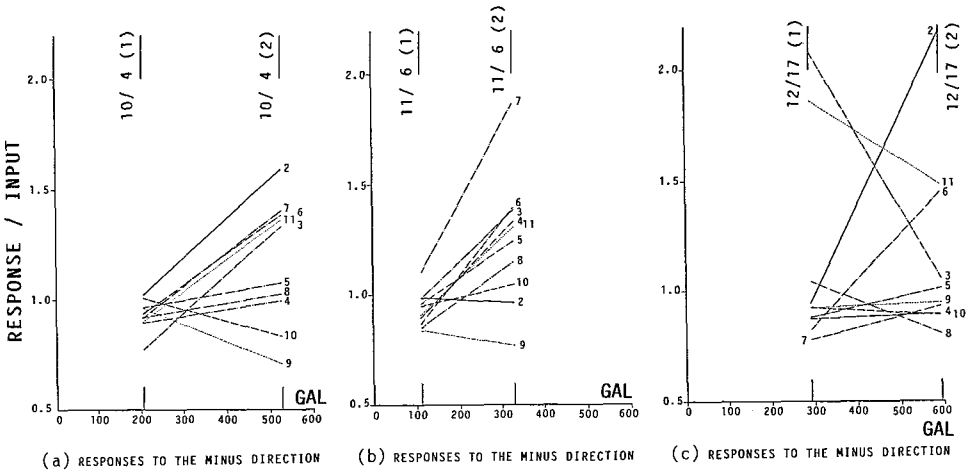

FIG.14-2: Magnifications of Response Accelerations in the case of "EARTHQUAKE EXCITATIONS"

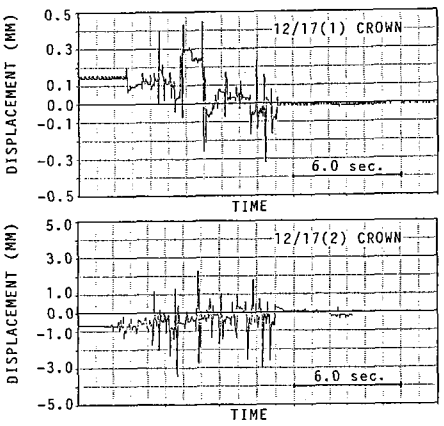

FIG.15:
Time Histories of Response Accelerations at CH.2 to "12/17(1)" and "12/17(2)"

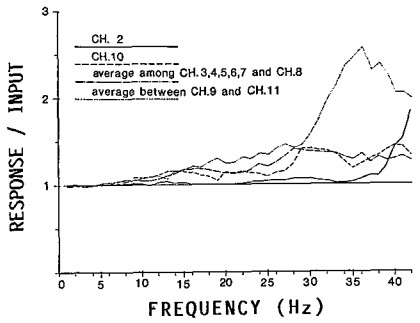

FIG.16: Resonance Curves

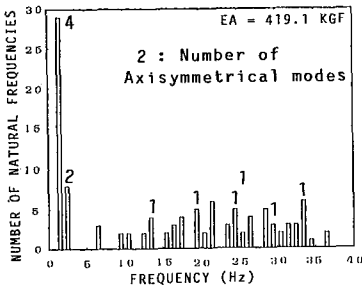

FIG.17: Histogram of Distribution of Natural Frequencies

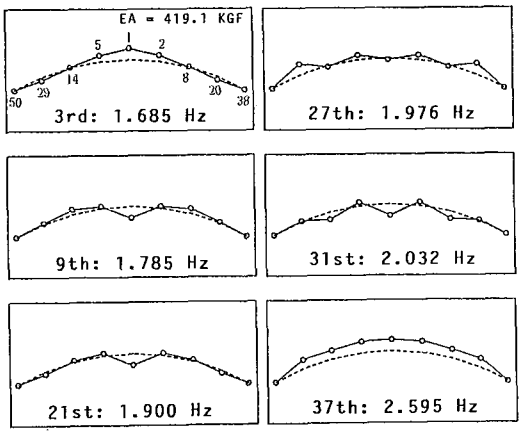

FIG.18: Axisymmetric Mode Shapes and the Natural Frequensies

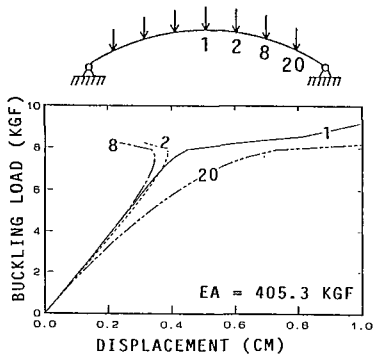

FIG.19: Load-Displacement Relation to Uniform Load

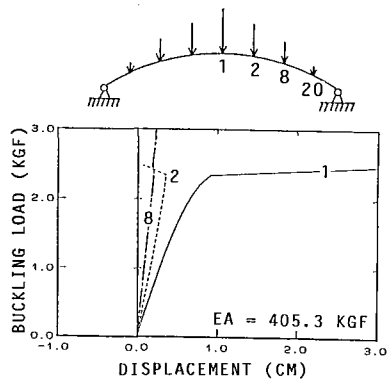

FIG.20: Load-Displacement Relation to Conical Load

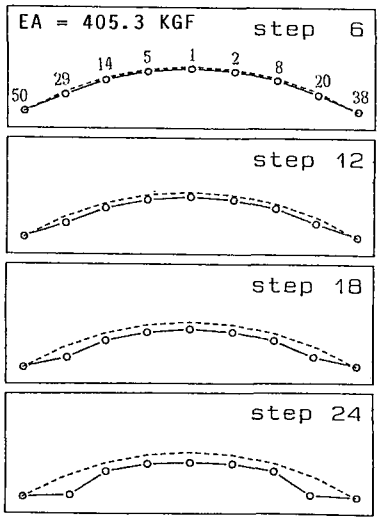

FIG.21: Progress of Deflection Mode to Uniform Load

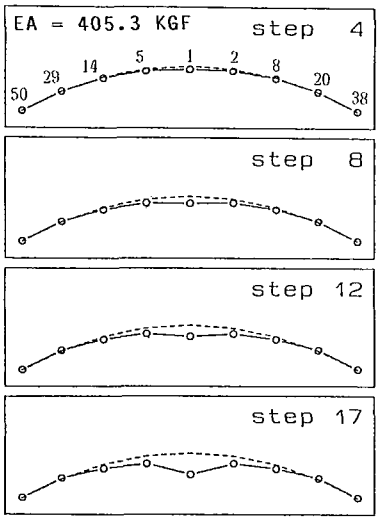

FIG.22: Progress of Deflection Mode to Conical Load

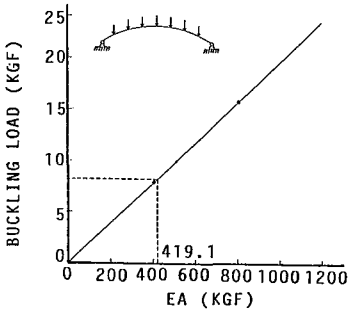

FIG.23: Relations between Buckling Load and (EA) in the case of Uniform Load

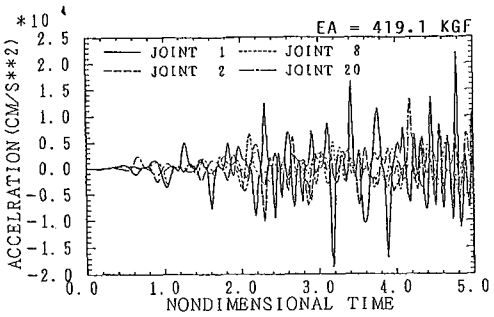

FIG.24(a): Time Histories of Response Accelerations at Joint Numbers of 1,2,8 and 20

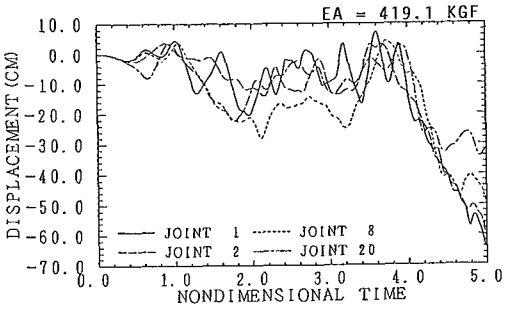

FIG.24(b): Time Histories of Response Displacements at Joint Numbers of 1,2,8 and 20

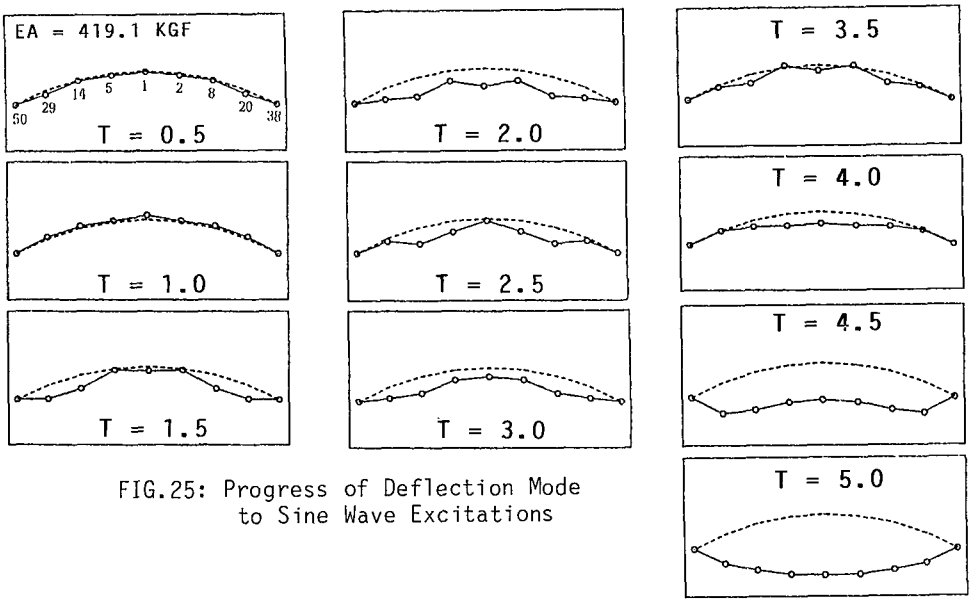

FIG.25: Progress of Deflection Mode to Sine Wave Excitations

TABLE 5: Comparison of Buckling Loads

	LOADING		BUCKLING LOAD (kgf)		EA (KGF)
TEST	DYNAMICALLY	SINE WAVE	TEST.DBL	52.7	533.1
			TEST.DBL(1)	43.6	
			TEST.DBL(2)	20.9	
THEORY	STATICALLY	UNIFORM LOAD	7.9		533.1
		CONICAL LOAD	2.3		
	DINAMICALLY	SINE WAVE	WITHIN 27.3		419.1